

Bloch and Néel disclination lines in a small-anisotropy ferromagnet

M. Kléman

Laboratoire de Physique des Solides,* Bâtiment 510, Université Paris-Sud, 91405 Orsay, France

(Received 11 June 1975)

Bloch and Néel lines are, from a topological point of view, disclinations in a spin lattice. They are described in a small-anisotropy ferromagnet ($K \ll 2\pi M_S^2$) for two different situations. First one considers Bloch lines at the limit of vanishing anisotropy: A complete calculation shows that cross and circular Bloch lines have no core singularity, which fact decreases exchange energy, and that stray fields control the size of cross Bloch lines, while magnetostriction controls the size of circular Bloch lines. Second one considers Néel lines in a situation inspired by recent experimental results on amorphous ferromagnets. Here it is shown that the interactions between lines, whose size is controlled by the existence of a small anisotropy, are mainly due to stray-field effects and magnetostriction effects. Topologically Bloch lines are wedge disclinations and Néel lines are twist disclinations. The importance of magnetostriction is emphasized throughout the article and original methods are given in an Appendix to calculate the internal magnetostrictive stresses due to singularities. Although the theoretical results do not coincide fully with the experimental ones, especially because a strictly two-dimensional calculation is used, we are confident that the analysis is true in the main. Qualitatively, this analysis differs drastically from the case $K \gg 2\pi M_S^2$.

I. INTRODUCTION

Up to now, singularities in ferromagnets have been studied mostly in the two following very different situations:

(a) Bloch lines on Néel walls in very thin films of low anisotropy ($q = K/2\pi M_S^2 \ll 1$). The configurations are dominated by stray-field effects; the well-known cross-tie walls are characteristic of such situations.¹

(b) Néel lines (commonly called Bloch lines also, but we prefer to reserve this terminology for the first situation described above) on 180° Bloch walls in high-anisotropy uniaxial materials ($q = K/2\pi M_S^2 \gg 1$). This is the typical situation encountered in "hard bubbles"²; an even number of Néel lines are disposed periodically on a circular Bloch wall. This equilibrium is determined by a competition between attractive stray-field effects (each line is charged) and repulsive exchange effects (see Fig. 1). Two typical lengths enter into the physics of this geometry: a Bloch-wall thickness $\delta_w = (A/K)^{1/2}$, where A is the exchange energy constant, and the exchange length of stray-field effects $\delta_s = (A/2\pi M_S^2)^{1/2}$. Because the stray-field effects are so small, one gets $\delta_s/\delta_w = q^{1/2} \gg 1$. The exchange effects of a singularity extend therefore over long distances, which explain their contribution to the general balance.

It appears today that, although Néel walls and Bloch lines in low- q materials have been thoroughly investigated, it is only in the case of bubbles in high- q materials that the notion of singularity has really attracted the attention of magneticians and that singularities have been studied as such.

In this paper, we plan to study singularities in

the low-anisotropy limit. It is a remarkable feature of this limit, which appears clearly when K is strictly zero, that spontaneous magnetostriction comes in as an important factor in the general balance of forces: The spin singularities act as sources of internal stresses. This is in fact an extension of a previous work in which we calculated the internal stresses created by simpler inhomogeneities, viz., walls^{3a} and wall junctions.^{3b} In this article, we calculate them for line singularities, and show that for $q \ll 1$ they contribute in an essential way to the stability of lines on a wall, since they are not masked by exchange effects between lines. The details of the calculation, which are not trivial, are given in a long Appendix. We consider this Appendix as an essential part of this paper, although this paper should be readable without a detailed study of the Appendix. Another point in this paper is that we insist on a presentation of singularities as distinct objects, and as such spin singularities in ferromagnets are *disclinations*. In our opinion,

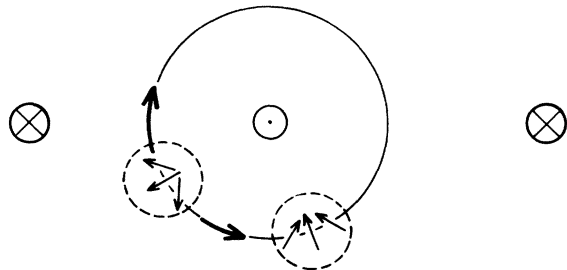


FIG. 1. Arrows indicate the direction of the magnetization in the middle of the wall. Néel lines in the centers of the dotted circles.

this concept has not yet got the status it deserves in the field of magnetism, although some attempts have been made.⁴ The main object of this paper is the specific properties of singularities in low- q ferromagnets, not with a general description of singularities in a vector field. However, some comments of a general nature are necessary, and we include them in this Introduction.

In any ordered material, the physical description of singularities necessitates the use of two kinds of concepts. First, the singularities are related to the geometrical invariance properties of the material, for example, in a solid crystal a dislocation is characterized by its Burgers's vector, equal to a vector of translation of the point lattice; in a nematic crystal a disclination is characterized by its rotation vector, whose direction and magnitude are such that the perfect nematic crystal is invariant under such a rotation. We refer to such properties as *topological properties*. Second, the energy of singularities must minimize some thermodynamic function and the distribution of the quantity which describes the variation of order [for example, the elastic displacement $\vec{u}(\vec{r})$ around a dislocation in a solid, or the angle $\phi(\vec{r})$ the magnetization makes with a fixed direction are such quantities] must obey some constitutive laws. Such properties, which imply some knowledge of the physical interactions in the material, we call *energetic properties*. Calculations resorting to these properties are, for example, those of line energy, mobilities, etc. Such a double point of view can be profitable in the study of ferromagnets. We introduce the term "spin lattice" by which we mean that there are some geometrical properties of invariance in the ground state of a spin system. Let us indicate some important topological and energetic features of ferromagnets.

Topological properties. On a macroscopic scale, a ferromagnet is a set of magnetic moments (spins) which can be described by a vectorial density $\vec{M}(\vec{r})$ depending continuously (except in a reduced number of points) on the position. In the ground state, all the spins are parallel and pointing in the same directions, which is a situation reminiscent of the nematic arrangement in liquid crystals, but different anyway, since in the latter case the director $\vec{n}(\vec{r})$ can point either way without any variation in the free-energy density. However, the analogy can be fruitful if one tries to give a general description of the singularities capable of occurrence in a spin "lattice."

The symmetries of the lattice are not locally broken in a smooth variation of the density $\vec{M}(\vec{r})$, but so they are in the vicinity of a singularity.

Singularities must be limited to small regions. These requirements constitute the true justifications of the Volterra process, well known in dislocation theory,⁵ by which it is shown that different types of singularities correspond to the different point symmetries (of translation and of rotation) of the lattice. For an illustration of this point of view in the case of liquid crystals, see Ref. 6. In ferromagnets, this leads us to consider Bloch and Néel lines as disclination lines of strength multiple of ± 1 (the magnetization rotates by an angle multiple of $\pm 2\pi$ when one follows a circuit enclosing the line). Disclinations are related to rotation symmetries. Lines of strength $\pm \frac{1}{2}$ are not topologically allowed since rotation symmetries by an angle of π do not exist for \vec{M} (they exist for the director \vec{n} in a nematic). Point singularities, which we shall not mention any more in this article, can also exist in ferromagnets, as they exist in nematics; their topological properties have been recently studied by Nabarro.⁷ It is worth mentioning that the spin lattice of ferromagnets is invariant in any translation of the spins. Therefore, dislocations of translation of not quantized Burgers's vectors are allowed in this lattice, but, if such a dislocation of Burgers's vector \vec{b} happens to exist, it can relax to $\vec{b}=0$ by emitting permitted dislocations of infinitesimal Burgers's vectors $d\vec{b}$ (except if some defect of the crystal lattice is able to pin it). The same situation is already known to hold in nematics,⁷ where dislocations of translation are viscously relaxed to zero.

Let us finally note that, in the language of disclinations, Bloch lines on Néel walls are *wedge* disclinations, which means that the rotation vector characteristic of the singularity is along the line; Néel lines on Bloch walls are *twist* disclinations, which means that the rotation vector defining the singularity is perpendicular to the line.

Energetic properties. They can differ widely for different media having the same symmetries, and consequently the same topological objects (in the sense indicated above) will demonstrate different physical properties in these different media. For example, because of the existence of an anisotropic coupling to the atomic lattice, spin configurations in a ferromagnet are characterized by Weiss domains and Bloch (or Néel) walls, and the singular lines are confined to stay in these walls. Ferromagnets with vanishing anisotropy K (amorphous ferromagnets with no long-range internal stresses) allow a more direct comparison between lines in ferromagnets and nematics. Even in that case, stray-field or magnetostriction effects might be the dominating terms in the observed configurations. There is nothing com-

parable in nematics.

The first part of this paper (Sec. II) is devoted to isolated wedge lines in an amorphous ferromagnet. In the second part (Sec. III), we shall consider the situation where $q = K/2\pi M_s^2$ is small compared to 1 and show that the balance between twist lines, in a particular geometry, is obtained through a competition between stray-field effects and magnetostriction effects. Most of the results we obtain are conjectural, but the model we shall use for Néel lines on Bloch walls is inspired by a recent experimental work on amorphous ferromagnets.⁸ In this article, our main intention is not to explain the model used in this recent work, but to use it as a starting point in order to develop considerations specific to low- q ferromagnets. As was already indicated, we shall insist on magnetostriction effects.

II. WEDGE LINES IN AN AMORPHOUS FERROMAGNET

Spin disclinations in ferromagnets are attended, at very small distances, by very large variations in exchange energy. Even in the case $K \neq 0$, it is conceivable that, in the core region itself, the major contribution comes from exchange energy and that stray-field effects come afterwards, as first-order perturbation terms.

Consider a straight wedge disclination, i.e., a line such that \vec{M} rotates by an angle $\pm 2\pi S$ about the axis of the line when moving along a circuit enclosing the line. The main topological possibilities correspond to (see Fig. 2): $S = +1$: the circular Bloch line, the radial Bloch line, the spiraling Bloch line; $S = -1$: the cross Bloch line.

Other possibilities will not be considered here. We discuss successively for these cases the exchange magnetostatic and magnetoelastic energies, as the main contributions to their energy.

A. Exchange energy

Let us first assume that the spins stay in planes perpendicular to the line and look for solutions which minimize exchange energy alone. The ex-

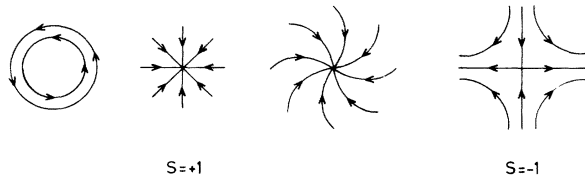


FIG. 2. Wedge disclinations. $S = +1$: the circular Bloch line, the radial Bloch lines, the spiraling Bloch line; $S = -1$: the cross Bloch line.

change energy density reads

$$F_{ex} = A(\nabla\vec{n})^2, \tag{1}$$

where $\vec{M} = M_s \vec{n} \cdot F_{ex}$ is minimized by

$$\nabla^2 \vec{n} = L(\vec{r})\vec{n} \tag{2}$$

where L is a position-dependent Lagrangian multiplier taking into account the constraint $\vec{n}^2 = 1$. If ϕ is the angle made by $\vec{M} (M_x, M_y, 0)$ with a constant direction in the x, y plane, and θ an azimuthal angle in this plane, one gets as singular solutions

$$\phi = S\theta + \phi_0, \quad S = \pm 1, \pm 2, \text{ etc.} \tag{3}$$

a formula already obtained for nematics.⁹ For $S = 1$, $\phi_0 = 0$ corresponds to the radial Bloch line and $\phi_0 = \frac{1}{2}\pi$ to the circular Bloch line. The line tension is given by

$$W_{ex} = 2\pi AS^2 \ln(r_0/a) + W_c, \tag{4}$$

where r_0 is an outer length (r_0 is, according to the case, a wall width, a distance between neighboring lines, etc.) and a is a lattice parameter. W_c is a core energy, necessary because the distribution (3) is singular for $r = 0$.

The line tension (4) is large and another solution, taking into account the possibility for \vec{M} to have a nonvanishing M_z component (cf. a similar problem for nematics^{10,11}) enables us to decrease it drastically, allowing even the singularity to disappear, if one imposes $M_x = M_y = 0$ for $r = 0$ (see Fig. 3). One gets, assuming $M_z = 0$ at a distance $r = r_0$, and cylindrical symmetry,

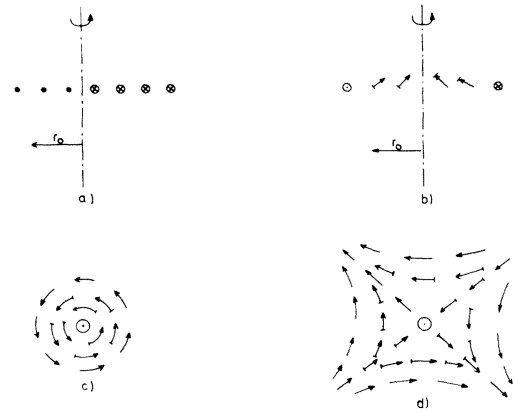


FIG. 3. The solution which minimizes the exchange energy in a Bloch line: (a)–(c) circular Bloch line; (d) cross Bloch line; (a) with a singularity on the core (meridian cut); (b) without a singularity on the core (meridian cut); (c) section perpendicular to the line (no core singularity); (d) section perpendicular to the line (no core singularity). The nail indicates a tilted axis and the arrow the direction of \vec{M} . Curved arrows indicate the lines of force of the projection of \vec{M} in the plane of drawing.

$$\left(\frac{r}{r_0}\right)^{2|S|} = \frac{1 - \sin\psi}{1 + \sin\psi}, \quad (5)$$

where ψ is the angle between \vec{M} and the z axis. The line tension therefore reduces to

$$W_{\text{ex}} = 2\pi|S|A. \quad (6)$$

This quantity is *independent* of r_0 and does not contain any singular terms. Using a terminology borrowed from the theory of disclinations, one would say that the core has split, and that the splitting occurs in all the volume offered to the line.

B. Magnetostatic energy

This is a nonlocal term. Let us first note that one can write $(\nabla\vec{n})^2$ [cf. Eq. (1)] as the sum of a "splay" term $(\text{div}\vec{n})^2$, a "twist" term $(\vec{n}\cdot\text{curl}\vec{n})^2$, and a "bend" term $(\vec{n}\times\text{curl}\vec{n})^2$:

$$F_{\text{ex}} = A[(\text{div}\vec{n})^2 + (\text{curl}\vec{n})^2]. \quad (7)$$

In this equation, we have neglected a term which integrates to a surface term, and therefore does not contribute to the bulk equilibrium. This decomposition (and the terminology) are borrowed from the theory of liquid crystals (see, for example, Refs. 9 and 12). As an illustration of this decomposition, note that the planar circular Bloch line is divergenceless (no splay term) and twistless, and that the planar radial Bloch line contains only splay. A Bloch wall contains only twist.

The splay term corresponds to a magnetic charge

$$\text{div}\vec{M} = -\rho, \quad (8)$$

and must be avoided as much as possible. This is the reason why the radial Bloch line $S = +1$ is forbidden; in this case $\text{div}\vec{n}$ is of a constant sign. On the other hand, circular Bloch lines are divergenceless. The radius of the circular Bloch line is therefore defined by a competition between anisotropy energy and exchange energy, i.e., typically is of the order of δ_w if $K \neq 0$. In an amorphous ferromagnet, the radius of a circular Bloch line depends on surface stray-field effects and magnetostriction.

In contradistinction with the circular Bloch line, the cross Bloch line ($S = -1$) is not divergenceless, but the total charge is zero. Its radius is therefore determined by a competition between bulk magnetic charges (quadrupolar) and exchange. One can therefore expect $r_0(S = -1) \approx \delta_s$. This latter relationship obtains by writing a balance equation between stray-field energy ($\sim 2\pi M_s^2$ per unit volume) and exchange energy. Some published calculations on isolated Bloch lines¹²⁻¹⁴ reach comparable conclusions.

C. Magnetostriction

We have developed elsewhere the general theory of internal stresses due to inhomogeneities in the magnetization distribution.³ One can introduce fictitious dislocation densities $\alpha_{ij}(\vec{r})$, which act as the sources of these internal stresses, and are related as follows to the magnetization $\vec{M} = M_s\vec{n}(\vec{r})$.

$$\alpha_{ij} = -\epsilon_{ijk}e_{ij,k}^0, \quad (9)$$

where $e_{ij}^0(r)$ are the symmetric local magnetostrictive distortions; they would be the only distortions present if \vec{M} were uniform. In a cubic ferromagnet, they read

$$e_{11}^0 = \frac{3}{2}\lambda_{100}n_1^2, \quad (10)$$

$$e_{12}^0 = \frac{3}{2}\lambda_{111}n_1n_2,$$

where λ_{100} and λ_{111} are the dimensionless coefficients of magnetostriction.

One realizes immediately, consulting Eq. (9), that the important sources of internal stresses are those regions where \vec{M} varies rapidly or is singular, i.e., walls,^{3a} wall junctions,^{3b} disclinations, and singular points. This last object will not be considered here.

Let us first consider a planar circular Bloch line. In cylindrical coordinates, the associated dislocation densities are

$$\alpha_{3\theta} = -(3/2r)\lambda_s, \quad (11)$$

where λ_s is an isotropic constant of magnetostriction. $\alpha_{3\theta}$ can be interpreted as a density of tilt walls terminating on the line (see Fig. 4) and giving rise to an over-all *elastic wedge disclination* of rotation vector

$$\Omega_3 = \int \alpha_{3\theta} r d\theta = -3\pi\lambda_s. \quad (12)$$

The reader is referred to Ref. 15 for a description

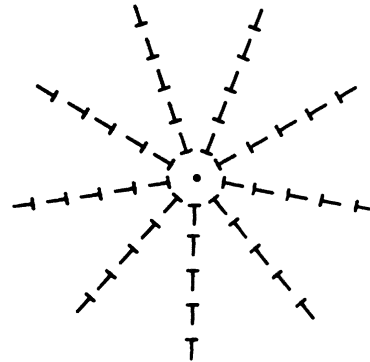


FIG. 4. Stresses due to a circular Bloch wall are those due to a constant density of tilt walls. Here these tilt walls are represented by edge dislocations.

of the elasticity of disclinations in solids.

The stresses due to the densities $\alpha_{3\theta}$ are singular on $r=0$. They are decreased if, once more, one assumes that \vec{M} has a nonvanishing M_z component. In fact, one can introduce a variable $\Omega_3(r)$

$$\Omega_3(r) = 3\pi\lambda_s \left(\sin^2\psi - r \frac{d\psi}{dr} \sin 2\psi \right), \quad (13)$$

which does not represent the whole internal stresses, but their largest sources.

As we do not wish to enter into the details of the calculation, we only note that these results indicate that we can estimate the magnetoelastic energy of a circular Bloch line as the energy of a disclination Ω_3 (for an upper limit), i.e.,

$$W_{me} \sim \mu r_0^2 \Omega_3^2. \quad (14)$$

(Here and in other places the suffix me stands for magnetoelastic.) This quantity is small compared to W_{ex} as long as r_0 does not reach values of the order of

$$\delta_{me} = \frac{1}{\lambda_s} \left(\frac{A}{\mu} \right)^{1/2},$$

i.e., $50 \mu m$ with $A = 10^{-6} \text{ dyn}$, $\mu = 10^{11} \text{ dyn/cm}^2$, $\lambda_s = 10^{-6} \text{ rad}$. This calculation assumes $K = 0$. If the anisotropy does not vanish the problem is quite different, as we shall see below.

For a planar cross Bloch line in an amorphous ferromagnet, one gets

$$\alpha_{3\theta} = (3/2r)\lambda_s \cos 4\theta; \quad (15)$$

$$\alpha_{3r} = (3/2r)\lambda_s \sin 4\theta.$$

Here, too, these sources of internal stresses are decreased by letting \vec{M} escape in the third dimension. Note that the analysis of the sources defined by Eq. (14) requires more complex elastic concepts than in the case of the circular Bloch line: there are no simple elastic disclinations, but for each value of θ the densities of Eq. (15) define a wall of dislocations. The internal stresses they create are discontinuous on the wall. This wall is a *Somigliana defect*. Hence the planar cross Bloch line appears as the boundary line of a density of Somigliana defects. However, we shall assume for the time being that the magnetostrictive line tension of a cross Bloch line is of the same order as the value found from Eq. (14). This is certainly true as long as $\delta_{me} \gg \delta_s$, δ_s being the typical dimension of a cross Bloch line.

This discussion of magnetostriction has assumed a perfectly cylindrical geometry of the magnetization around the Bloch line. This is not the case except if K is strictly zero and if there is no anisotropy of any kind. But cross Bloch lines, even for $K = 0$, have a finite dimension δ_s , which

leads us to think that such objects are necessarily embedded in regions where the magnetization is practically uniform. The simplest way of conceiving such a requirement is to reintroduce walls, at least in the vicinity of cross Bloch lines (Fig. 5).

In other words, as regards magnetostriction, the dislocation densities introduced above are limited to finite regions and are, moreover, screened at the wall boundaries by opposite densities. They are, therefore, very little effective, except inside the lines. Pursuing the analysis, we are led to distinguish these internal effects, which we know are weak anyway because of the core splitting, from long-range stresses; for their evaluation we can simplify the geometry as follows: We consider a wall of thickness $2d$ (Fig. 6) and a region of vanishing thickness inside the wall, on which the magnetization changes abruptly; this represents, in place of the Bloch line, a small Bloch wall perpendicular to the wall. The lines of force of \vec{M} are assumed circular. One gets in the axes drawn in Fig. 6

$$\begin{aligned} \alpha_{31} &= \frac{3\pi}{4d} \lambda_s \sin \frac{\pi y}{d} - \frac{3}{4} \lambda_s \sin \frac{\pi y}{d} \delta(x), \\ \alpha_{32} &= \frac{3\pi}{4d} \lambda_s \cos \frac{\pi y}{d} [U(x) - U(-x)], \end{aligned} \quad (16)$$

where $U(x)$ is the step function [$U(x > 0) = 1$; $U(x < 0) = 0$]. α_{31} and α_{32} vanish outside the wall.

The long-range stresses created by the densities of Eq. (16) can be calculated in details by a method we shall use in a subsequent paragraph for a different case. Here we shall content ourselves in noting that the only densities which are liable to give rise to important stresses at long distances are those related to the $\delta(x)$ term. We can overestimate them by replacing this term by a dislocation dipole. α_{31} represents a dislocation density whose Burgers's vector is along x , and whose direction is along z (edge dislocation). Integrating

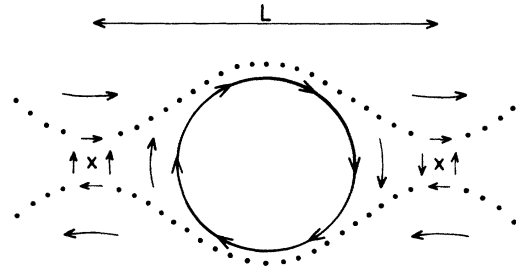


FIG. 5. Cross Bloch lines in an amorphous ferromagnet are dimensionally limited, but circular Bloch lines are not. Here is pictured a possible situation satisfying the first requirement. The dashed lines represent the "wall" boundaries.

α_{31} in the range $0 < y < d$, one gets for the Burgers's vector

$$b = -\frac{3}{4}(d/\pi)\lambda_S. \quad (17)$$

Assuming $d \sim 10^{-5}$ cm, $\lambda_S \sim 10^{-5}$, one gets $b \sim 10^{-9}$ cm, i.e., a value typically ten times smaller than a crystal dislocation Burgers's vector. But note also that d , which is small for a cross Bloch line ($d = \delta_S$), can be very large for a circular Bloch line. The line tension, using Nabarro's formula for a dipole,¹⁶ amounts to

$$W_{mc} = \frac{9\mu}{32\pi^3} \frac{d^2\lambda_S^2}{1-\nu} \left(\ln \frac{4}{3} \frac{\pi}{\lambda_S} - 1 \right). \quad (18)$$

The stresses decrease with distance like r^{-2} . Successive Bloch lines along a Néel wall act as dipoles of alternating signs.

Consider, therefore, a wall, as depicted in Fig. 5, and assume that $K=0$. The relevant energy terms are:

(i) from the cross Bloch lines: $2\pi A/L$ per unit length of wall. The factor 2 takes into account the fact that the cross Bloch line is charged; we assume that there is an equal contribution to the total energy from exchange ($\pi A/L$) than from stray fields. The magnetostriction term is negligible since δ_S is so small;

(ii) from the circular Bloch line:

$$\frac{\pi A}{L} + \frac{9\mu}{32\pi^3} \frac{d^2\lambda_S^2}{(1-\nu)L} \left(\ln \frac{4}{3} \frac{\pi}{\lambda_S} - 1 \right),$$

where d is the radius of the line;

(iii) from the triangular regions between the lines, where we have exchange energy and magnetostatic energy. Using a dimensional analysis, one gets $\alpha(A/d) + \beta M_S^2 L$, where α and β are numerical coefficients.

When minimizing the total energy (in an approximate way), one finds that the presence of the magnetostrictive term determines the dimension of the circular Bloch line ($d \sim \delta_{mc}$), while the presence of the magnetic poles in the triangular regions leads to a value of L the smallest possible. Hence the lines $S = +1$ and $S = -1$ must be in close contact. A more precise discussion would be worthwhile, in which a two-dimensional array of lines

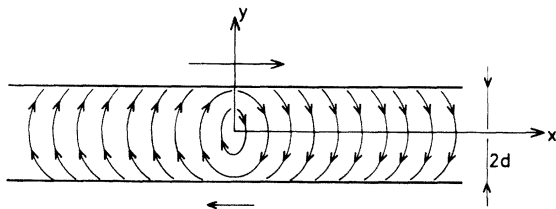


FIG. 6. Model of the circular Bloch line used to calculate the long-range stresses it creates.

should be introduced, and its stability discussed.

But in summary we can conclude that, for $K=0$, while the width of a Bloch line is controlled by stray fields, the width of a circular Bloch line is controlled by magnetostriction.

For $K \neq 0$, the argument has to be modified. For in this latter case a third length occurs in the problem, which is the wall thickness δ_w . It seems probable that two cases now occur, whether the value of the dimensionless parameter $p = \delta_w^2/\delta_{mc}^2 = \mu\lambda_S^2/K$ is smaller or larger than unity.

$p > 1$. The wall thickness is large. One is led to the conclusion that magnetostriction will control the size of circular Bloch lines, as in the situation already described.

$p < 1$. The wall thickness is small, and the typical configuration is in the form of cross-tie walls, where the size of circular Bloch lines is of the order of δ_w . The size of cross Bloch lines is still of the order of δ_S .

III. TWIST LINES IN A SMALL-ANISOTROPY FERROMAGNET

In this section we intend to show that twist-line stability (Néel lines on Bloch walls) depends essentially on a competition between magnetostrictive and stray-field effects in low- q materials. First we recall some general features of the topology of twist lines. Then we discuss the possible occurrence of twist lines in low- q materials with regard to the experimental work of Puchalska and Sadoc.⁸ Finally we calculate the exchange, magnetostrictive, and stray-field effects in a geometry of zig-zag walls with twist lines at the tips of the zig-zag.

A. Topology of twist lines

This topology has been described in details by Nabarro⁷ and we just recall the two most important situations encountered in 180° Bloch walls.

(i) Twist line perpendicular to the direction of \vec{M} in the adjacent domains (Fig. 7). As indicated by Rault,¹⁷ this model is not devoid of twist ($\vec{n} \cdot \text{curl} \vec{n} \neq 0$), but largely avoids the effects of splay: two small zones are not divergenceless

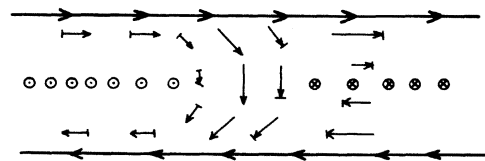


FIG. 7. Néel (twist) line. The spin rotation is right handed in the left part of the figure, and left handed in the right part (nail convention).

($\text{div } \vec{n} \neq 0$) but are of opposite signs; the line acts as a magnetic dipole. There is no singularity on \vec{M} here. This Bloch line is well known in platelets with parallel anisotropy.

(ii) Twist line parallel to the direction of \vec{M} in the adjacent domains (Fig. 8). The deformation is essentially bendlike ($\vec{n}_\perp \text{ curl } \vec{n} \neq 0$). The magnetostatic effects are strong, since the charges on the segment AB are all of the same sign. Nevertheless, this situation is very frequently encountered in high- q materials ($q > 1$) when the axis of anisotropy is perpendicular to the specimen; recently, such lines have even been seen in low- q materials.⁸

There is no singularity anywhere on the line, and the geometry is symmetric with respect to AB . This symmetry is conserved if one tilts the walls with respect to a direction perpendicular to AB (Fig. 9). This is the geometry we shall study in the remainder of this article, assuming that such lines appear periodically along parallel zig-zag walls (Fig. 10).

B. Important comments on the geometry of Fig. 10 in low- q materials

The geometry of Fig. 10 has been inferred from Bitter experiments⁹ on Co-P amorphous electro-deposited platelets. The thicknesses T of the platelets range from $12 \mu\text{m}$ to $38 \mu\text{m}$, the periodicity of the zig zags from $S \sim 2 \mu\text{m}$ to $S \sim 4 \mu\text{m}$, the angle θ_0 from 50° to 70° , and the distance D between parallel walls from 5 to $13 \mu\text{m}$. The material possesses a small uniaxial anisotropy ($K \sim 1.7 \times 10^4 \text{ erg/cm}^3$) giving an easy axis perpendicular to the plate thickness. The saturation magnetization M_s is of the order of 700 G, and the exchange constant $A \sim 0.4 \times 10^{-6} \text{ erg/cm}$. These values are from Ref. 18. They lead to $q = K/2\pi M_s^2 \sim 0.03$.

Uniaxial materials with perpendicular easy axis are well known to display striped domains. Few theoretical efforts have been made in order to understand stripes in high- q materials,^{19,20} i.e.,

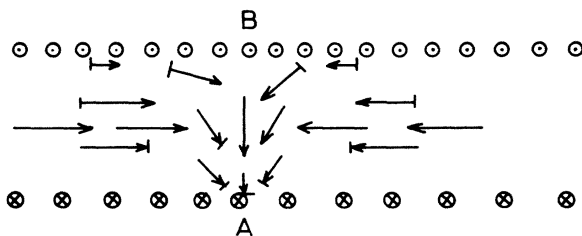


FIG. 8. Néel (twist) line. The spin rotation is right handed in the left part of the figure, and left handed in the right part.

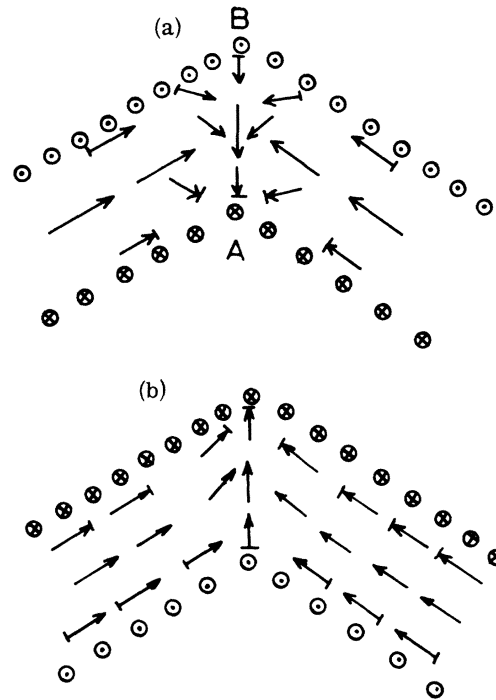


FIG. 9. Same as in Fig. 8, but tilted along AB . Fig. 9(b) corresponds to a more favorable situation than Fig. 9(a), because of a smaller exchange energy.

materials for which the demagnetizing effects due to the stray fields at the surface are so small that it is possible to assume that $\vec{M}(x, y)$ does not depend on the z coordinate. In such a case striped domains appear at any thickness. Under an applied perpendicular field, they transform to bubble domains.² The stripes repeat distance $2D$ is approximated (for large q) by

$$D \sim T^{1/2}(\pi^2 AK)^{1/4}(2\pi M_s^2)^{-1/2}. \tag{19}$$

More work has been done when q is small. In such a case, it is clear that the stable situation at vanishing thicknesses is \vec{M} lying "in the plane." It is only above a critical thickness T_c that striped domains can appear. According to Murayama,²⁰

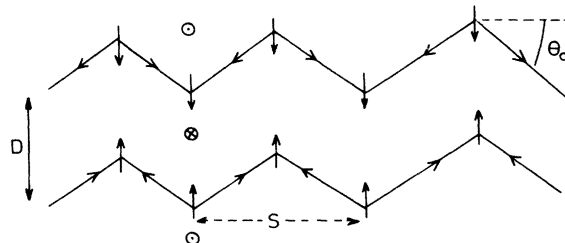


FIG. 10. Direction of the magnetization in the middle of the wall is figured out. See text for other comments.

this critical thickness is of the order of the wall thickness

$$T_c = 2\pi(A/K)^{1/2} \quad (20)$$

while the critical repeat distance $2D_c$ is given by

$$D_c \sim T_c. \quad (21)$$

For $T > T_c$, in Murayama's model, the repeat distance increases with T according to the law

$$D = T^{1/2}(\pi^2 A / 2\pi M_S^2)^{1/4}, \quad (22)$$

which differs from Eq. (19) by a renormalizing factor $q^{-1/4}$.

Murayama's calculation takes into account the possibility for \vec{M} to depend on z . In fact, his method includes the well-known μ^* correction of Williams *et al.*²¹ and puts into evidence the eventual existence of flux-closure configurations inside each stripe. An experimental illustration of this property of flux closure can be found in Ref. 22 (iron single-crystal thin foils).

These flux-closure zones, which are not in the form of closure domains, or this μ^* correction take place in the vicinity of the surface, in a thickness typically of the order of δ_S .²⁴ In the inner zone the magnetization fluctuates with a maximum amplitude $\phi_0(T)$ depending on the thickness. For large thickness (i.e., large compared to T_c), \vec{M} reaches practically the easy-axis direction, and the stripes turn to true domains separated by walls²⁵; in fact, this asymptotic behavior of stripes also appears on Eq. (22), which is the equation obtained by Kittel²⁶ for the flux-closure pattern containing true closure domains in low- q materials. This result is not surprising. Note also that Eq. (22) does not seem to be violated by the experimental results of Puchalska and Sadoc.⁸ This comment cannot be made more specific because of the necessary impreciseness of these measurements, as well as the large possible fluctuations on the physical constants involved.

In conclusion, the treatment of the magnetic pattern of Fig. 10 can be done (qualitatively but not quantitatively; some quantitative features would have to be reconsidered, if for example there are some true closure domains and if the walls are oblique to the plane) with the assumption that \vec{M} does not depend on z , but the discussion we have done implies much more. The relationship between D and T is given by Eq. (22), which does not take into account the existence of a zig-zag shape of the walls, as well as a fine distribution of \vec{M} inside the walls. This seems reasonable indeed.

(a) Any fluctuation of the surface magnetic free poles involving a periodicity *along* the stripes does not couple magnetostatically with the stripes

(see Appendix A). Hence, the periodicity of the zig-zag is independent of D .

(b) The zig-zag depends, therefore, on the distribution of the magnetic poles in the walls and in a strip of amplitude $\frac{1}{2}S \tan\theta_0$, and on exchange and magnetoelastic terms related to the inhomogeneities of \vec{M} in the walls. The magnetoelastic terms linked to the layer of thickness δ_S on the surfaces are small compared to those in the walls, because δ_S is so small in low- q materials.

(c) As regards the magnetic poles (see Fig. 11), the contributions due to the regions outside the wall and those due to the singularities at the apexes of the zig-zag are of very different orders of magnitude.

The poles in the triangles of surface $\frac{1}{2}S^2 \tan\theta_0$ (see Fig. 11) are spread with a density of the order of qM (μ^* correction). Along the Néel lines the total charge is $(8dM/\pi)T$, where d is half the wall width and T the thickness of the sample. Let us compare these two contributions. One gets

$$\frac{\sigma_t}{\sigma_N} = \frac{q}{32} \frac{S^2}{dT} \tan\theta_0. \quad (23)$$

This is of the order of $q \tan\theta_0$ if one uses the experimental values and is therefore small.

In other words, the only poles contributing to the general equilibrium of the zig-zag come from the Bloch lines. We study in the next subsections the different contributions to the zig-zag pattern.

C. Exchange energy and exchange interactions

According to the argument developed for the case of wedge lines, the exchange line tension is of the order of πA . There is no core energy.

A typical dimension of the line is still δ_S . Now $\delta_S \ll \delta_w$, since q is so small. Therefore, exchange interactions between lines are small. It is likely that Fig. 9(b) is more favorable than Fig. 9(a) from the point of view of exchange energy. Hence in Fig. 10 one has assumed the strengths of successive lines are equal in sign (compare with Fig. 1). But the relative signs of the successive lines on a wall are irrelevant in the general stability of the pattern. The total contribution of the exchange energy is, per unit length of wall along the x axis,

$$W_{\text{exch}} = 2\pi A/S,$$

where S is the distance between lines (Fig. 10).

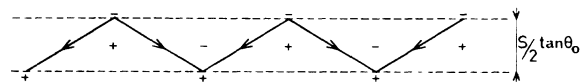


FIG. 11. Magnetic free poles contributing to the zig-zag shape.

We shall not use S any more as a symbol indicating the strength of a line (see Sec. II) so there should be no confusion.

D. Magnetostriction

Exchange energy playing no role in the stability, one has to look to magnetostriction. Appendix B is devoted to a complete calculation of this term for *one* zig-zag tip, i.e., a dihedron with infinite half-planes. The complete zig-zag is the sum of such dihedra alternating in signs (see Fig. 12, from which it is apparent that the extra half-walls cancel).

In Appendix B, one shows that the quasidislocation densities attached to the zig-zag wall divide in two parts: a part which is a density spread along the walls and a part which is an edge dislocation localized along the Néel line, of Burgers's vector $b \sim -(3/2\pi)\lambda_S d \sin\theta_0$ [Eq. (B15)]. The zig-zag pattern is defined by two independent variables: the repeat distance S and the angle θ_0 , let us say. A virtual displacement of θ_0 (at S constant) corresponds to the work of a virtual force along y , to which the most important contribution comes from the tips of the zig-zag. This force can be estimated by the Peach-Koehler formula²³ for the edge dislocation localized along the Néel line. The virtual displacement at θ_0 constant is taken into account by minimizing the total energy with respect to S .

We need

$$e_{11} = \frac{3}{2} \frac{\lambda_S d}{\pi} \sin\theta_0 \sum \pm \frac{\sin\phi}{r}$$

[see Eq. (B9)] for insertion in the Peach-Koehler formula [Eq. (B16)]. We want to calculate this expression in point A (see Fig. 12), i.e., for $x=0$, $y = \frac{1}{4}S \tan\theta_0$. The only dihedra contributing are localized along the row at $y = -\frac{1}{4}S \tan\theta_0$. We get

$$\sum \pm \frac{\sin\phi}{r} = \frac{S}{2} \tan\theta_0 \sum_{n=-\infty}^{n=+\infty} \frac{1}{[\frac{1}{2}S + (n-1)S]^2 + \frac{1}{4}S^2 \tan^2\theta_0} = \frac{\pi}{2S} \tanh\left(\frac{\pi}{2} \tan\theta_0\right). \tag{24}$$

The summation of this series is classical; use, for example, the γ -function properties (Ref. 27, p. 264).

The Peach-Koehler force F_y^{mc} in A is equal, for the line of length T , to

$$F_y^{mc} = \frac{3}{4} \mu \lambda_S^2 d^2 (T/S) \sin^2\theta_0 \tanh\left(\frac{1}{2}\pi \tan\theta_0\right). \tag{25}$$

This term is repulsive.

The energy of magnetostriction of a wall can be calculated from the $e_{ij}(r)$. It is reasonable to assume that parallel zig-zag walls do not interact; this is because the periodicity D is large com-

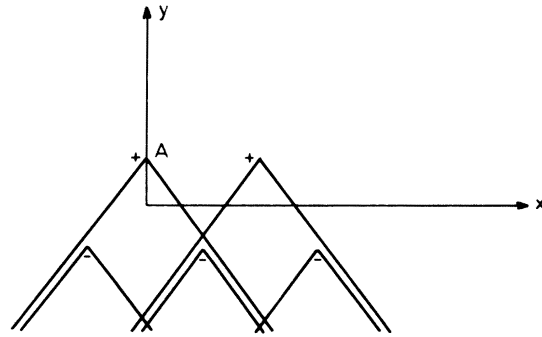


FIG. 12. Dihedra of infinite half-planes alternating in signs constitute the true magnetoelastic zig zag.

pared to the amplitude of the zig-zag. This calculation, which is not reported here, gives the following *order of magnitude* (per unit length of wall along the x axis):

$$W_{mc} = \mu \lambda_S^2 \frac{d^2}{S} T \left(\sin^2\theta_0 + \frac{d^2}{S^2} \frac{1}{\cos^2\theta_0} \right). \tag{26}$$

The first term arises from the terms in $1/r$ [see (B9)] and the second from the terms in r^{-2} [see (B9)].

E. Stray-field energy

We first calculate the potential V of the magnetic free poles in A (see Fig. 12), assuming that all the magnetic free poles in the different Néel lines are concentrated at points, with charges $e = \pm(8d/\pi)M_S T$, where d is the wall thickness. The stray-field interaction energy is therefore $W_S = eV$ per line, and the configurational force exerted on a line by the stray fields of the others is

$$F_y^S = \pm \frac{\partial eV}{\partial y} = \pm \frac{2}{S} \frac{\partial (eV)}{\partial (\tan\theta_0)};$$

the sign is such that the force is attractive.

The calculation is done in Appendix C. One finds [Eq. (11)]

$$F_y^S = -\frac{64}{\pi} \left(\frac{d}{S}\right)^2 M_S^2 T^2 \frac{1}{(\tan\theta_0)^{1/2}} \exp(-2\pi \tan\theta_0). \tag{27}$$

F. Balance of the different contributions

Apart from the contributions which have been calculated, one has to add the wall energy, which reads

$$W_w = \frac{(AK)^{1/2}}{\cos\theta_0} T$$

per unit length of wall along x . W_w contributes to the configurational force along the Néel line. We

evidently have

$$F_y^w = -2(AK)^{1/2} T \sin\theta_0. \quad (28)$$

The balance of the configurational forces reads

$$F_y^{\text{mc}} + F_y^S + F_y^w = 0. \quad (29)$$

These contributions are of different orders of magnitude *a priori*, according to the experimental values of M_S , μ , λ_S , A , and K . Let us note that F_y^S and F_y^w are of the same sign. The presence of the magnetostrictive term F_y^{mc} is therefore *necessary* in order to obtain an equilibrium. But its numerical coefficient is small compared to F_y^S and F_y^w :

$$\left| \frac{F_y^{\text{mc}}}{F_y^S} \right| = \frac{9\pi}{256} \frac{\mu\lambda_S^2}{M_S^2} \frac{S}{T} g(\theta_0) \sim 2 \times 10^{-5} \frac{S}{T} g(\theta_0),$$

$$\left| \frac{F_y^{\text{mc}}}{F_y^w} \right| = \frac{9}{4} \frac{\mu\lambda_S^2}{(AK)^{1/2}} \frac{A}{K} \frac{1}{S} f(\theta_0) \sim 1.3 \times 10^{-2} \frac{d}{S} f(\theta_0).$$

This imposes necessarily $g(\theta_0)$ large, i.e., θ_0 large, as well as S/T . This is possible, since making $\tan\theta_0$ large reduces F_y^S by a large factor. But a similar argument cannot be used for the competition between F_y^{mc} and F_y^w . We are therefore led to the necessary following conclusions:

(a) The role of magnetostriction is compulsory: This is the only term which is repulsive. Exchange interaction between Néel lines could also be repulsive, but small because of $q \ll 1$. The only possibly repulsive term which has been neglected is that one due to magnetic free poles in the triangular regions, but it must be small too. If these structures exist in strictly zero magnetostriction material, their equilibrium would involve this magnetostatic effect, neglected here.

(b) The wall surface tension is certainly overestimated in Eq. (28) if one chooses for K the experimental value of Ref. 18. This would lead indeed to a value of $S \sim 10^{-2} d$, which is too small by three orders of magnitude. But note that there are large fluctuations in the measurements of K done on electrodeposited platelets, attended by large fluctuations in the measurements of M_S .²⁹ Also it is possible that the walls are not truly 180° walls, but that \vec{M} oscillate on a smaller angular range, as in ordinary striped domains. This point needs further experimental and theoretical research, but at the moment internal consistency of the theory we present leads to drop F_y^w in Eq. (29), as if $K=0$ as in a true amorphous material. In such a case the only contribution to the wall tension would come from magnetostriction [Eq. (26)]:

$$F_y^w = -4\mu\lambda_S^2 \frac{d^2}{S} T \tan\theta_0 \left(\cos^4\theta_0 + \frac{d^2}{S^2} \right). \quad (30)$$

(c) The magnetization distribution proposed in

Fig. 10 is not the only one compatible with the observations; the existence of a zig-zag does not mean that there is necessarily a Néel line at the tip. If such a Néel line does not exist, the sense of rotation of the spins on both sides of the tip is the same and there are no magnetic poles. The stray-field effect disappears completely. But even if there is no Néel line, the magnetostrictive terms, etc., are practically of the same order of magnitude³⁰ as when the Néel line exists for large value of θ_0 . They, however, have to vanish for $\theta_0=0$. Now a balance is possible between magnetostrictive terms of different signs [repulsive: Eq. (25); attractive: Eq. (30)], if $K=0$. But it is clear *a priori* that such an equilibrium cannot be stable against a general flattening of the wall. Hence we are led to reject this model, and to attribute the stability of the geometry to the presence of the Néel lines, through their stray-field effects.

Let us now consider the solutions of Eq. (29), assuming $K=0$. We get approximatively

$$2 \cdot 10^{-5} (S/T) \sin^2\theta_0 \tanh\left(\frac{1}{2}\pi \tan\theta_0\right) \\ \times (\tan\theta_0)^{1/2} \exp(2\pi \tan\theta_0) = 1,$$

that is,

$$S/T \sim 2 \text{ (for } \theta_0 = 50^\circ \text{)}$$

$$\text{(experimental value } S/T = \frac{1}{6} \text{)},$$

$$S/T \sim 10^{-4} \text{ (for } \theta_0 = 70^\circ \text{)},$$

$$\text{(experimental value } S/T \sim 10^{-1} \text{)}.$$

Although the variation of S/T is correctly obtained, the orders of magnitude are drastically different. Here too we can think that it does not invalidate our main arguments. For small values of S/T , S and T are both small, and interactions between the two surfaces and between parallel walls should be taken into account. For large values of S and T , the contributions from the triangular regions have to be taken into account (the component of \vec{M} normal to the plate becomes more important), and screen the mutual magnetostatic interactions of the Néel lines, which would result in a decrease of the exponential behavior. We, therefore, stay confident in this result that the balance is due to a competition between magnetostatic and magnetostrictive terms. Also, the experimental results show a large dispersion.⁸

Finally we have obtained here only one equation of minimization (that one relative to $\tan\theta_0$). Virtual variations of S lead to the other one.

IV. CONCLUSIONS

In this article we have studied two opposite situations relative to small anisotropy ($K/2\pi M_S^2 \ll 1$)

ferromagnets. In the first one, we assume that the spin singularities are wedge lines (Bloch lines) and show that the sizes of such singularities are controlled by different mechanisms according to the strength of the singularity for cross Bloch lines by stray field effects and for circular Bloch lines by magnetostriction. In the second one, the spin singularities are twist lines whose mutual arrangement has been suggested by experimental results. Here too the theory puts into evidence the importance of stray-field effects and magnetostriction effects.

These magnetostriction effects are typical of small-anisotropy ferromagnets. The geometries are difficult to calculate because the small anisotropy allows the magnetization to vary in the three dimensions, in order to decrease as much as possible stray-field effects. Such three-dimensional variations are well known in striped domains in which a complete calculation, although attempted,^{20, 22} has never led to a correct fitting between experiment and theory. In this article we have not attempted a three-dimensional calculation and the experimental and theoretical results are still harder to reconcile; but we are confident that the main mechanisms we have described are the correct ones.

ACKNOWLEDGMENTS

The author is grateful to Dr. I. B. Puchalska for discussion about her experimental results and to Professor J. Friedel for comments. He is indebted to Dr. J. Miltat for critical reading of the manuscript.

APPENDIX A: PERIODIC SURFACE MAGNETIC POLES

Let us start from the classical striped domains, and assume first that each stripe bears constant magnetic poles, which only change sign from one stripe to the other (Fig. 13). Note σ , the surface magnetic poles density. According to Maxwell's equations, the potential Φ obeys the following relationships:

in the bulk:

$$\nabla^2 \Phi = 0;$$

on the surface:

$$\left(\frac{\partial \Phi}{\partial z} \right)_{z=+0} = -2\pi\sigma \tag{A1}$$

$$\Phi(z = +0) = \Phi(z = -0) .$$

Then we have, expanding $\sigma(xy)$ in Fourier series, and using an index 0 for the configuration of Fig. 13

$$\sigma_0(x, y) = \frac{4}{\pi} \sigma_0 \sum_{n=1}^{\infty} \frac{\sin nq_0 y}{n} , \tag{A2}$$

Hence

$$\Phi_0 = \frac{8\sigma_0}{q_0} \sum_{n=1}^{\infty} \frac{\sin nq_0 y}{n^2} e^{-nq_0 z} \text{ (for } z > 0) . \tag{A3}$$

The magnetostatic energy is given by

$$W_0 = \frac{1}{2} \int \sigma_0(x, y) \Phi_0(z=0) dx dy . \tag{A4}$$

Let us now perturb this configuration by adding a periodic density of magnetic free poles:

$$\Delta\sigma = \sum_{m,p} A_{mp} e^{imq_0 y} e^{ipqx} , \tag{A5}$$

where m and p are integers running from $-\infty$ to $+\infty$. One keeps the same periodicity along y . Owing to the linearity of Maxwell's equations, the variation in potential $\Delta\Phi$ is readily calculated:

$$\Delta\Phi = 2\pi \sum \frac{A_{mp}}{k_{mp}} e^{imq_0 y} e^{ipqx} e^{k_{mp}z} , \tag{A6}$$

where

$$k_{mp} = (p^2 q^2 + m^2 q_0^2)^{1/2} . \tag{A7}$$

The total energy reads

$$W = W_0 + \frac{1}{2} \int (\sigma_0 \Delta\Phi + \Phi_0 \Delta\sigma) dx dy + \frac{1}{2} \int \Delta\sigma \Delta\Phi dx dy .$$

We are interested in the interaction energy

$$\begin{aligned} W_I &= \frac{1}{2} \int (\sigma_0 \Delta\Phi + \Phi_0 \Delta\sigma) dx dy \\ &= 16 i \pi^2 \frac{\sigma_0}{q_0} \sum_{n=0}' \frac{A_{n,0}}{n^2} \end{aligned}$$

where the summation \sum' excludes $n=0$.

This expression immediately tells us that the interaction energy depends only on those components

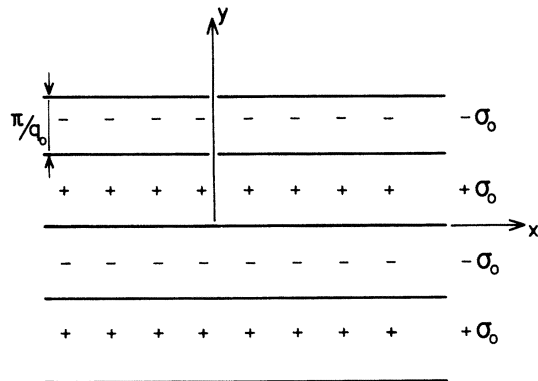


FIG. 13. Surface distribution of the magnetic free poles.

of $\Delta\sigma$ which do not fluctuate along x . The others are completely decoupled. The periodicity of the fluctuations along x is independent (magnetostatically) from the periodicity of the stripes.

APPENDIX B: MAGNETOSTRICTIVE SELF-STRESSES AND SELF-CURVATURES OF A NÉEL LINE

The geometry which is considered is pictured in Fig. 14(a). Each half-wall is first calculated in its own axes [Fig. 14(b)], then the distortions and curvatures obtained are transformed to the axes xyz linked to the Néel line [Fig. 14(a)]: $\pm\theta_0$ is the angle of the wall with the x direction. The direction of \vec{M} in the middle of each wall is indicated on the figure, as well as outside the walls, which are perfect Bloch walls all over their length and thickness, except along the segment AB . Here the magnetization abruptly changes direction.

The calculation of the stresses and curvatures (bend-twist) are made first for a slice of wall of thickness dy_p (measured along AB), located at P . This is the reason why we choose the XYZ axes to be mobile with P . We use the formulas obtained by Kléman^(3b) for a half-wall. The results are afterwards summed over AB .

Then, we calculate the energy of the singularity. In a second part, we calculate the interactions between Néel lines. All the frames of reference are right handed.

Distribution of \vec{M}

For the left half-wall

$$M_x = M \cos\theta; \quad M_z = M \sin\theta$$

$$\theta = (\pi/2d)y_p \cos\theta_0; \quad -\frac{1}{2} < \theta < +\frac{1}{2}\pi.$$

For the right half-wall (in different XYZ axes) the same formulas correspond,

Left half-wall, slice of thickness dy_p

We first evaluate the quasiplastic stresses $\Delta\sigma_{ij}^0$ for this slice, then the stresses and curvatures (bend-twist) in the axes XY . The only nonvanishing quasielastic distortions are

$$e_{11}^0 = \frac{3}{2} \lambda_S \cos^2\theta;$$

$$e_{13}^0 = \frac{3}{2} \lambda_S \sin\theta \cos\theta;$$

$$e_{33}^0 = \frac{3}{2} \lambda_S \sin^2\theta.$$

Then, if we orient the slice along the $+y$ direction [according to the "FSRH" (finish start, right hand) convention of de Witt¹⁵ for orienting the singularities, the line is here oriented along the

positive z direction], we get

$$\Delta e_{11}^0 = +\frac{3}{2} \lambda_S \sin 2\theta \Delta\theta = -a(\theta, \Delta\theta),$$

$$\Delta e_{33}^0 = +a(\theta, \Delta\theta), \quad (B1)$$

$$\Delta e_{13}^0 = -\frac{3}{2} \lambda_S \cos 2\theta \Delta\theta = -c(\theta, \Delta\theta).$$

Using the notations of Ref. 8, one gets

$$E_{11} = -a, \quad E_{33} = +a, \quad E_{22} = E_{12} = E_{32} = 0,$$

$$E_{31} = -c, \quad \Omega_1 = \Omega_2 = \Omega_3 = 0.$$

Note that because of the vanishing of the Ω_j , this slice of wall does not introduce any rotation between the domains θ and $\theta + \Delta\theta$ which it separates. The E_{22} distortion is put arbitrarily equal to zero, which introduces a nonvanishing σ_{22}^+ stress at infinity. But this can be adjusted afterwards if necessary. One gets finally (Ref. 3b)

$$\Delta e_{11}^+ = -\frac{a}{2\pi} \varphi^l, \quad \Delta e_{12}^+ = -\frac{a}{4\pi} (1 + \ln\rho),$$

$$\Delta e_{22}^+ = 0, \quad \Delta e_{23}^+ = -\frac{c}{4\pi} (1 + \ln\rho), \quad (B2)$$

$$\Delta e_{33}^+ = +\frac{a}{2\pi} \varphi^l, \quad \Delta e_{31}^+ = -\frac{c}{2\pi} \varphi^l,$$

where φ^l and ρ are polar coordinates in the XYZ frame of reference [Fig. 14(b)] l is for left. One chooses the determination $-\pi < \varphi^l < +\pi$.

The nonvanishing bend-twist components are given by

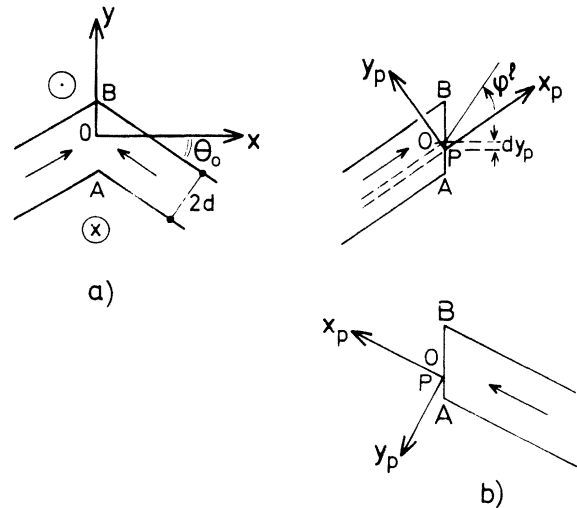


FIG. 14. Geometry of a spin singularity at a wall junction. Fixed (x, y) and mobile axes (x_p, y_p) .

$$\Delta K_{11}^+ = -(c/2\pi\rho) \cos\varphi^i, \quad \Delta K_{21}^+ = -(c/2\pi\rho) \sin\varphi^i \quad (\text{B3})$$

$$\Delta K_{13}^+ = +(a/2\pi\rho) \cos\varphi^i, \quad \Delta K_{23}^+ = +(a/2\pi\rho) \sin\varphi^i$$

They are such that, by definition, the variation $d(\Delta\omega_i^+)$ of curvature of the lattice between two points χ_i and $\chi_i + d\chi_i$ is given by

$$d(\Delta\omega_i^+) = K_{ji}^+ d\chi_j^+.$$

Now the same quantities in the fixed axes xyz read (we drop the superscript +):

$$\begin{aligned} \Delta e_{11} &= -(a/2\pi) \cos\theta_0 [\varphi^i \cos\theta_0 - (1 + \ln\rho) \sin\theta_0], \\ \Delta e_{22} &= -(a/2\pi) \sin\theta_0 [\varphi^i \sin\theta_0 + (1 + \ln\rho) \cos\theta_0], \\ \Delta e_{12} &= -(a/4\pi) [\varphi^i \sin 2\theta_0 + (1 + \ln\rho) \cos 2\theta_0], \\ \Delta e_{13} &= -(c/2\pi) [\varphi^i \cos\theta_0 - \frac{1}{2}(1 + \ln\rho) \sin\theta_0], \\ \Delta e_{23} &= (c/2\pi) [-\varphi^i \sin\theta_0 - \frac{1}{2}(1 + \ln\rho) \cos\theta_0], \\ \Delta e_{33} &= +(a/2\pi) \varphi^i. \end{aligned} \quad (\text{B4})$$

$$\begin{aligned} \Delta K_{11} &= -(c/2\pi\rho) \cos\theta_0 \cos(\varphi^i + \theta_0), \\ \Delta K_{12} &= -(c/2\pi\rho) \sin\theta_0 \cos(\varphi^i + \theta_0), \\ \Delta K_{13} &= +(a/2\pi\rho) \cos(\varphi^i + \theta_0), \\ \Delta K_{21} &= -(c/2\pi\rho) \cos\theta_0 \sin(\varphi^i + \theta_0), \\ \Delta K_{22} &= -(c/2\pi\rho) \sin\theta_0 \sin(\varphi^i + \theta_0), \\ \Delta K_{23} &= +(a/2\pi\rho) \sin(\varphi^i + \theta_0), \\ \Delta K_{31} &= \Delta K_{32} = \Delta K_{33} = 0. \end{aligned} \quad (\text{B5})$$

Right half-wall, slice of thickness dy_p

Similarly to the left half-wall, we first obtain the e_{ij}^0 . The slice is oriented along Y . One obtains the right half-wall by simply rotating the left half-wall and changing signs.

$$\begin{aligned} \Delta e_{11}^0 &= -\frac{3}{2}\lambda_s \sin 2\theta \Delta\theta = +a(\theta, \Delta\theta), \\ \Delta e_{33}^0 &= -a(\theta, \Delta\theta), \\ \Delta e_{13}^0 &= +\frac{3}{2}\lambda_s \cos 2\theta \Delta\theta = +c(\theta, \Delta\theta). \end{aligned}$$

One therefore gets

$$E_{11} = +a, \quad E_{33} = -a, \quad E_{31} = -c.$$

Going now to the fixed axes xyz , one gets, with obvious changes of notation:

$$\begin{aligned} \Delta e_{11} &= (a/2\pi) \cos\theta_0 [\varphi^r \cos\theta_0 + (1 + \ln\rho) \sin\theta_0], \\ \Delta e_{22} &= +(a/2\pi) \sin\theta_0 [\varphi^r \sin\theta_0 - (1 + \ln\rho) \cos\theta_0], \\ \Delta e_{12} &= (a/4\pi) [-\varphi^r \sin 2\theta_0 + (1 + \ln\rho) \cos 2\theta_0], \\ \Delta e_{13} &= (c/2\pi) [-\varphi^r \cos\theta_0 - \frac{1}{2}(1 + \ln\rho) \sin\theta_0], \\ \Delta e_{23} &= (c/2\pi) [\varphi^r \sin\theta_0 - \frac{1}{2}(1 + \ln\rho) \cos\theta_0], \\ \Delta e_{33} &= -(a/2\pi) \varphi^r. \end{aligned} \quad (\text{B6})$$

$$\begin{aligned} \Delta K_{11} &= +(c/2\pi\rho) \cos\theta_0 \cos(\varphi^r - \theta_0), \\ \Delta K_{12} &= -(c/2\pi\rho) \sin\theta_0 \cos(\varphi^r - \theta_0), \\ \Delta K_{13} &= +(a/2\pi\rho) \cos\theta_0 \cos(\varphi^r - \theta_0), \\ \Delta K_{21} &= +(c/2\pi\rho) \cos\theta_0 \sin(\varphi^r - \theta_0), \\ \Delta K_{22} &= -(c/2\pi\rho) \sin\theta_0 \sin(\varphi^r - \theta_0), \\ \Delta K_{23} &= +(a/2\pi\rho) \sin(\varphi^r - \theta_0). \end{aligned} \quad (\text{B7})$$

Distortions of the singularity

They read, for each slice $\Delta\theta$, corresponding θ_0 , a given point P :

$$\begin{aligned} \Delta e_{11} &= (a/2\pi) [(1 + \ln\rho) \sin 2\theta_0 + (\varphi^r - \varphi^i) \cos^2 \theta_0], \\ \Delta e_{22} &= -(a/2\pi) [(1 + \ln\rho) \sin 2\theta_0 - (\varphi^r - \varphi^i) \sin^2 \theta_0], \\ \Delta e_{12} &= -(a/4\pi) (\varphi^i + \varphi^r) \sin 2\theta_0, \\ \Delta e_{13} &= -(c/2\pi) (\varphi^i + \varphi^r) \cos\theta_0, \\ \Delta e_{23} &= (c/2\pi) [(\varphi^r - \varphi^i) \sin\theta_0 - (1 + \ln\rho) \cos\theta_0], \\ \Delta e_{33} &= (a/2\pi) (\varphi^i - \varphi^r). \end{aligned}$$

Let us now introduce the polar angle φ' in the axes $x'y'z'$ with origin P parallel to the fixed axes xyz with origin O . The quantities $\varphi^i - \varphi^r$, $\varphi^i + \varphi^r$ express simply as functions of φ' and θ_0 , modulo constant angles depending on the various determinations of φ' . But \int_a, \int_c sum up to zero when integrated on the wall thickness. Therefore in the final results these constant angles do not appear, and we may write, without caution

$$\varphi^i + \varphi^r = 2\varphi',$$

$$\varphi^i - \varphi^r = 0.$$

We therefore have

$$e_{11} = \frac{\sin 2\theta_0}{2\pi} \int a \ln \rho, \quad e_{22} = -e_{11}, \quad e_{33} = 0,$$

$$e_{12} = -\frac{\sin 2\theta_0}{\pi} \int a \varphi', \quad e_{13} = -\frac{\cos \theta_0}{\pi} \int c \varphi',$$

$$e_{23} = -\frac{\cos \varphi_0}{2\pi} \int c \ln \rho,$$

where a and c are the differential forms defined in Eq. (B1).

The evaluation of these equations can be done as follows: In the complex plane xyz let us introduce the complex number $\rho e^{i\varphi'}$ (Fig. 15). One has

$$\begin{aligned} \rho e^{i\varphi'} &= z - z_P \\ &= z - iy_P \\ &= -\frac{id}{\pi \cos \theta_0} \left(2\theta_0 - \frac{i\pi}{d} \cos \theta_0 z \right) \end{aligned}$$

where z is the affix of $M(x, y)$.

The integrals we need are simply related to the integrals

$$J = \int (\ln \rho + i\varphi') \cos 2\theta d\theta,$$

$$K = \int (\ln \rho + i\varphi') \sin 2\theta d\theta.$$

Writing $V = (i\pi/d) \cos \theta_0 z$, $x = 2\theta$, one gets

$$J = \frac{1}{2} \int_{-\pi}^{+\pi} \ln(x+V) \cos x dx,$$

$$K = \frac{1}{2} \int_{-\pi}^{+\pi} \ln(x+V) \sin x dx. \quad (\text{B8})$$

We integrate by parts

$$J = -\frac{1}{2} \int_{-\pi}^{+\pi} \frac{\sin x}{x+V} dx,$$

$$K = \frac{1}{2} \ln \frac{V+\pi}{V-\pi} + \frac{1}{2} \int_{-\pi}^{+\pi} \frac{\cos x dx}{x+V},$$

and look for the long-range stresses ($|V| \gg x$).

One therefore gets $J \sim \pi/V^2$; $K \sim \pi/V$, i.e.,

$$\int a \varphi' = \frac{3\lambda_s d}{2 \cos \theta_0} \frac{\cos \varphi}{r};$$

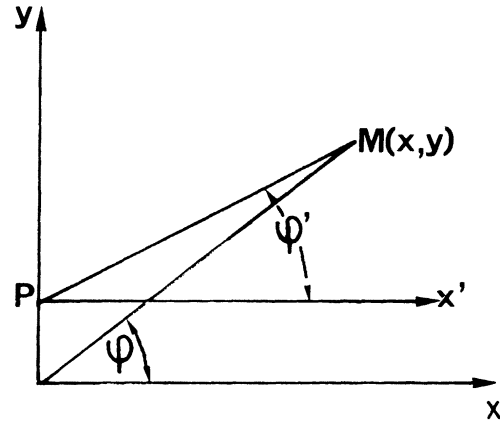


FIG. 15. Fixed (x, y) and mobile axes (x', y') along the junction AB of Fig. 14.

$$\int a \ln \rho = \frac{3\lambda_s d}{2 \cos \theta_0} \frac{\sin \varphi}{r},$$

$$\int c \varphi' = \frac{3\lambda_s d^2}{2\pi \cos^2 \theta_0} \frac{\sin 2\varphi}{r^2};$$

$$\int c \ln \rho = -\frac{3\lambda_s d^2}{2\pi \cos^2 \theta_0} \frac{\cos 2\varphi}{r^2},$$

where r and φ are the polar coordinates of $M(x, y)$ in the axes xyz . Finally we get the following expressions of the distortions due to the Néel line

$$e_{11} = \frac{3}{2} \frac{\lambda_s d}{\pi} \sin \theta_0 \frac{\sin \varphi}{r},$$

$$e_{22} = -e_{11},$$

$$e_{33} = 0, \quad (\text{B9})$$

$$e_{12} = -\frac{3}{4\pi} \lambda_s d \sin \theta_0 \frac{\cos \varphi}{r},$$

$$e_{31} = -\frac{3\lambda_s d^2}{2\pi^2} \frac{1}{\cos \theta_0} \frac{\sin 2\varphi}{r^2},$$

$$e_{32} = +\frac{3\lambda_s d^2}{4\pi^2} \frac{1}{\cos \theta_0} \frac{\cos 2\varphi}{r^2}.$$

For $\theta_0 = 0$ (straight wall),³¹ the dominating terms are of the same nature than those due to a "dipole" of dislocations. This is very similar to the result obtained for a Bloch line (see main text) but the dipole dislocations are of a different nature than for the Bloch line (see below). For the Néel line, a dislocation term appears as soon as $\theta_0 \neq 0$, but at the same time the dipolar term increases and becomes catastrophic for $\theta_0 = \frac{1}{2}\pi$; a double wall [Fig. 16(a)] with a Néel line at its tip is unstable versus magnetostriction. A process of bulging

[Fig. 16(b)] would reduce the magnetostriction term. There is some evidence that "hard bubbles" nucleate easily at the end of double walls³² and such an instability we describe can be at their origin (apart from important magnetostatic effects).

Bend-twist curvatures of the singularity

They read, for each slice

$$\Delta K_{11} = -c/\pi\rho \cos\theta_0 \cos\varphi',$$

$$\Delta K_{21} = -c/\pi\rho \cos\theta_0 \sin\varphi'$$

All the other curvatures vanish.

We need to calculate $\int (c/\rho) \cos\varphi'$, $\int (c/\rho) \sin\varphi'$. These integrals are related, as its real and imaginary parts, to the complex integral $\int c/(z-z_p)$, which can be calculated from

$$\frac{dJ}{dz} = \int \frac{\cos 2\theta}{\rho e^{i\varphi'}} d\theta \simeq -\frac{2i\pi^2}{V^3} \frac{\cos\theta_0}{d}. \quad (\text{B10})$$

From these expressions, one gets

$$K_{11} = \frac{3}{\pi^2} \lambda_s \frac{d^3}{\cos\theta_0} \cos\varphi \frac{1-2\cos 2\varphi}{r^3}, \quad (\text{B11})$$

$$K_{21} = \frac{3}{\pi^2} \lambda_s \frac{d^3}{\cos\theta_0} \sin\varphi \frac{1+2\cos 2\varphi}{r^3}.$$

These rotations are most important for $\theta_0 \sim \frac{1}{2}\pi$, and do not vanish for the straight Bloch wall ($\theta_0 = 0$); if d is large enough they should be visible in Lang's topography.

Quasidislocation densities equivalent to the singularity

The calculation we have presented of the distortions and curvatures of a Néel line uses in a direct way the results obtained by Kléman^{3b} for a half-wall. An evaluation can also be made starting from

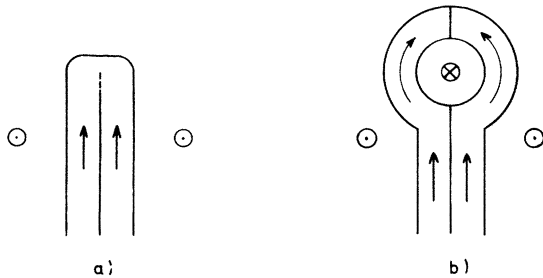


FIG. 16. Magnetostriuctive bulging at the tip of a double wall facilitates the nucleation of hard bubbles.

the quasidislocations equivalent to the singularity. This way we have used, in the main text, to estimate the magnetoelastic role of a Bloch line. Of course a calculation of the type presented in this appendix could have been done, and would have led to more accurate results, since the quasidislocations considered were restricted to the terms in the form of a Dirac function. We intend to do the same approximate calculation, using the α_{ij} densities, for the Néel line.

In the XYZ axes, the left half-wall magnetization has components

$$M_x = M \cos(\pi Y/2d) U(Y \tan\theta_0 - X),$$

$$M_z = M \sin(\pi Y/2d) U(Y \tan\theta_0 - X),$$

where $U(X)$ is the Heaviside step function

$$U(X) = \begin{cases} 1, & X > 0 \\ 0, & X < 0. \end{cases}$$

Transforming to the xyz axes, one gets

$$M_x = M \cos[(\pi/2d)(y \cos\theta_0 - x \sin\theta_0)] \cos\theta_0 U(-x),$$

$$M_y = M \cos[(\pi/2d)(y \cos\theta_0 - x \sin\theta_0)] \sin\theta_0 U(-x),$$

$$M_z = M \sin[(\pi/2d)(y \cos\theta_0 - x \sin\theta_0)] U(-x). \quad (\text{B12})$$

The same calculation for the right half-wall gives

$$M_x = -M \cos[(\pi/2d)(y \cos\theta_0 + x \sin\theta_0)] \cos\theta_0 U(x),$$

$$M_y = M \cos[(\pi/2d)(y \cos\theta_0 + x \sin\theta_0)] \sin\theta_0 U(x),$$

$$M_z = +M \sin[(\pi/2d)(y \cos\theta_0 + x \sin\theta_0)] U(x), \quad (\text{B13})$$

and we can formally write the total distribution by adding B12 and B13.

Now we need the $e_{ij}^0 = \frac{3}{2} \lambda_s n_i n_j$, from which we obtain the dislocation densities⁸

$$\alpha_{ij} = -\epsilon_{ikl} e_{ij,k}^0. \quad (\text{B14})$$

We shall content ourselves here in calculating those parts only in α_{ij} which are of the Dirac function type, and which come from the derivative $dU/dx = \delta(x)$. They arise from the following e_{ij}^0 ,

$$e_{12}^0 = \frac{3}{2} \lambda_s \sin\theta_0 \cos\theta_0 \cos^2\theta [U(-x) - U(x)],$$

$$e_{13}^0 = \frac{3}{2} \lambda_s \cos\theta_0 \sin\theta \cos\theta [U(-x) - U(x)];$$

hence for the α_{ij}

$$\begin{aligned}\alpha_{21} &= \frac{3}{2}\lambda_s \cos\theta_0 \sin 2\theta\delta(x) , \\ \alpha_{31} &= -\frac{3}{2}\lambda_s \sin 2\theta_0 \cos^2\theta\delta(x) .\end{aligned}\quad (\text{B15})$$

Because $\sin 2\theta$ changes sign along the segment AB , α_{21}^0 represents a dislocation dipole term (but see just below); α_{31}^0 is an edge dislocation of Burgers' vector $b = -(3d/2\pi)\lambda_s \sin\theta_0$ (by averaging on the segment AB). It is very interesting to notice that these dislocations resemble those inferred from the distortion tensor (B9), calculated (in another way) by using all the densities α_{ij} , and not only those pertaining to the segment AB solely. Some comments are necessary:

(a) First of all, let us note that the dislocations (B15) do not satisfy the so-called "node" condition $\alpha_{ii,i} = 0$. This means that it is necessary (at least for α_{21} , since $\alpha_{31,3} = 0$), to complement them, topologically, with a part at least of the densities we have dropped, and which are not localized on AB .

(b) Secondly, let us remark that the total "dipole" term behaves in $1/\cos\theta_0$, and not in $\cos\theta_0$ (B15). The densities which are dropped in (B15) are representative of the half-walls (Somigliana de-

fects), and play here a drastic role. But their contribution depends also deeply on the real length of the segments joining consecutive singularities. Hence, in order to calculate the stresses due to a zig-zag wall the length of these segments is the dominating term at long distances.

On the other hand, the α_{31} dislocation of Eq. (B15) provides us with the main term necessary if one wishes to calculate the configurational force exerted on a zig-zag wall by a set of stresses σ'_{ij} . The Peach Koehler formula²³

$$f_l = \sigma'_{ij} \epsilon_{jhl} \alpha_{hi} \quad (\text{B16})$$

tells us that such σ'_{ij} 's exert a point force on the singularity itself

$$f_l = \sigma'_{ij} \epsilon_{j3l} b; \quad b = \frac{3}{2}\lambda_s d \sin\theta_0$$

which are certainly dominant with respect to the force densities in the Somigliana walls.

Line tension of a singularity

We start from Eq (B9) and write the energy density as

$$\frac{1}{2}\sigma_{ij} e_{ij} = \frac{9\mu}{2\pi^2} \lambda_s^2 d^2 \frac{\sin^2\theta_0}{r^2} \left((\sin^2\varphi + \frac{1}{4}\cos^2\varphi) + \frac{d^2}{\pi^2 \cos^2\theta_0 r^4} (\sin^2 2\varphi + \frac{1}{4}\cos^2 2\varphi) \right).$$

After integration, one gets

$$W = \frac{45}{16} \mu \frac{\lambda_s^2 d^2}{\pi^2} \left(\sin^2\theta_0 \ln \frac{R}{d} + \frac{1}{2\pi^2 \cos\theta_0} \right). \quad (\text{B17})$$

APPENDIX C: MAGNETOSTATIC INTERACTION BETWEEN NÉEL LINES

The geometry is pictured Figs. 11 or 12. The magnetic free poles in the triangular regions between the zig zags are neglected. The magnetic free poles of a Néel line amounts to

$$e = \pm (8d/\pi)M_s T, \quad (\text{C1})$$

where d is the wall width and T the sample thickness. The calculation is done assuming that this charge is concentrated in a point in the middle plane of the specimen. The potential therefore reads

$$V = e \sum_{-\infty}^{+\infty} \frac{1}{r_n}, \quad (\text{C2})$$

where

$$\begin{aligned}r_n^2 &= S^2 \left[\left(n - \frac{1}{2} \right)^2 + \frac{1}{4} \tan^2\theta_0 \right] \\ &= \frac{1}{4} S^2 \left[(2n-1)^2 + \tan^2\theta_0 \right].\end{aligned}\quad (\text{C3})$$

The configurational force for the Néel line of length T reads

$$F_y^S = e \frac{\partial V}{\partial y} = -e^2 \frac{S}{2} \tan\theta_0 \sum \frac{1}{r_n^3}, \quad (\text{C4})$$

which can also be written

$$F_y^S = + \frac{2e}{S} \frac{\partial V}{\partial(\tan\theta_0)}, \quad (\text{C5})$$

The summation in Eq. (C2) can be put in the form of an integral by using the Cauchy formula for complex integrals.²⁸ Consider a region in the complex plane bounded by a curve γ (see Fig. 17). γ includes a circle of radius R which we shall make infinite; the two poles $z = \pm i \tan\theta_0$ of the complex function $f(z) = (z^2 + \tan^2\theta_0)^{-1/2}$ are left "outside" of γ . Because of the pole at $z = -i \tan\theta_0$, z changes argument by an angle of π when one describes γ from A to B . Hence $f(z)$ changes sign from A to B . Also note that the residue of f vanish at the poles, and that $|zf(z)| \rightarrow 1$ when

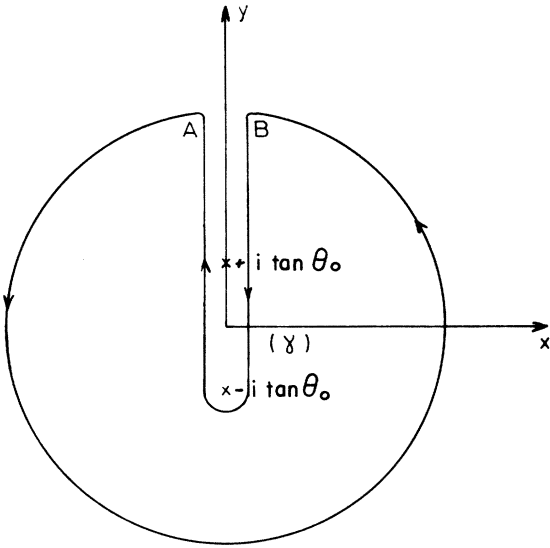


FIG. 17. Integration of Eq. (C2) (see text).

$z \rightarrow \infty$.

Now we have

$$\oint_{\gamma} \pi f(z) \cot(\pi z) dz = 2i\pi [f(s) + f(-1) + f(2) + f(-2) + \dots]$$

$$\oint_{\gamma} \pi f(z) \frac{1}{\sin \pi z} dz = 2i\pi [-f(1) - f(-1) + f(2) + f(-2) + \dots]$$

where we have in the right members the residues of the integrand for the poles $z = \pm n$ of $\cot \pi z$ and $1/\sin \pi z$. Hence

$$\oint_{\gamma} \pi f(z) \frac{\cos \pi z - 1}{\sin \pi z} dz = 4i\pi \sum_{p=-\infty}^{+\infty} f(2p-1) = 2 \frac{i\pi}{e} VS \quad (C6)$$

which reads also

$$V = + \frac{ie}{2S} \oint_{\gamma} f(z) \tan \frac{\pi z}{2} dz \quad (C7)$$

The contribution to this integral from the circle of radius R is imaginary when $R \rightarrow \infty [\tan \frac{1}{2}\pi z \rightarrow i; f(z) \rightarrow \pm 1/z$. It must therefore be equal to zero since V is real. We are left with the contribution from the segment along the y -axis

$$V = \pm \frac{e}{S} \int_{\tan \theta_0}^{\infty} \frac{\tanh \pi y dy}{(y^2 - \tan^2 \theta_0)^{1/2}} \quad (C8)$$

which, by a straightforward change of variable, reads

$$V = \pm \frac{e}{S} \int_1^{\infty} \frac{\tanh(\pi u \tan \theta_0) du}{(u^2 - 1)^{1/2}} \quad (C9)$$

Therefore

$$F_y^S = \pm 2\pi \frac{e^2}{S^2} \int_1^{\infty} \frac{[1 - \tanh^2(\pi u \tan \theta_0)] u du}{(u^2 - 1)^{1/2}} \quad (C10)$$

But the argument $\pi u \tan \theta_0$ is large, due to the magnitude of $\tan \theta_0$. We write

$$1 - \tanh^2(\pi u \tan \theta_0) \sim 4e^{-2\pi u \tan \theta_0},$$

$$F_y^S \sim \pm 8\pi \frac{e^2}{S^2} \int_1^{\infty} \frac{e^{-2\pi u \tan \theta_0} u du}{(u^2 - 1)^{1/2}} \quad (C10)$$

This is an integral which adds up to

$$F_y^S = \pm 8\pi (e^2/S^2) K_1(2\pi \tan \theta_0) \quad (C10)$$

where K_1 is the modified Bessel function of the second kind. Since $2\pi \tan \theta_0$ is large, one may write

$$K_1(2\pi \tan \theta_0) \sim \frac{1}{2} (1/\tan \theta_0)^{1/2} e^{-2\pi \tan \theta_0}.$$

Finally we get

$$F_y^S = \pm \frac{64}{\pi} \left(\frac{d}{S}\right)^2 M_S^2 T^2 \frac{1}{(\tan \theta_0)^{1/2}} e^{-2\pi \tan \theta_0} \quad (C11)$$

*Associé au Centre National de la Recherche Scientifique.

¹H. W. Fuller and M. E. Hale, *J. Appl. Phys.* **31**, 238 (1960).

²A. H. Bobeck, *Bell. Syst. Tech. J.* **46**, 1901 (1967); J. C. Slonczewski, *J. Appl. Phys.* **45**, 2705 (1974).

³(a) M. Kléman and M. Schlenker, *J. Appl. Phys.* **43**, 3184 (1972); (b) M. Kléman, *J. Appl. Phys.* **45**, 1377 (1974).

⁴See, for example, C. P. Bean, *Europhysics Conference on Disclinations*, 1972 (unpublished); M. Kléman, *Philos. Mag.* **22**, 739 (1970).

⁵J. Friedel, *Dislocations* (Pergamon, New York, 1964); F. R. N. Nabarro, *Theory of Crystal Dislocations* (Oxford U. P., England, 1967).

⁶J. Friedel and M. Kléman, in *Fundamental Aspects of Dislocation Theory*, NBS Spec. Pub. No. 317 (U. S. GPO, Washington, D. C., 1970), p. 607.

⁷F. R. N. Nabarro, *J. Phys.* **33**, 1089 (1972).

⁸I. B. Puchalska and J. F. Sadoc (unpublished).

⁹F. C. Frank, *Discuss. Faraday Soc.* **25**, 1 (1958).

¹⁰P. E. Cladis and M. Kléman, *J. Phys.* **33**, 591 (1972).

¹¹R. B. Meyer, *Philos. Mag.* **27**, 405 (1973).

¹²P. G. De Gennes, *The Physics of Liquid Crystals*, (Oxford U. P., England, 1974).

¹³E. Feldtkeller and H. Thomas, *Phys. Kondens. Mater.* **4**, 8 (1965).

¹⁴H. Bäurich, *Phys. Status. Solidi.* **16**, K39 (1966).

¹⁵R. de Witt, *J. Research Nat. Bur. Stand. A* **77**, 49

- (1973); 77, 359 (1973).
- ¹⁶F. R. N. Nabarro, *Adv. Phys.* 1, 271 (1952).
- ¹⁷J. Rault, *J. Phys.* 33, 383 (1972).
- ¹⁸G. S. Cargill, III, R. J. Gambino, and J. J. Cuomo, *IEEE Trans. Mag.* 803 (1974).
- ¹⁹Z. Malek and V. Kambersky, *Czech. J. Phys.* 21, 416 (1958); K. Kooy and U. Enz, *Philips Res. Rep.* 15, 7 (1960).
- ²⁰Y. Murayama, *J. Phys. Soc. Jpn.* 21, 2253 (1966).
- ²¹M. J. Williams, R. M. Bozorth, and W. Shockley, *Phys. Rev.* 75, 155 (1949).
- ²²A. Bourret and M. Kléman, *Phys. Status Solidi.* 23, 207 (1967); M. Kléman and A. Bourret, *Bull. Soc. Franc. Minér.* 23, 207 (1968).
- ²³M. Peach and J. S. Koehler, *Phys. Rev.* 80, 436 (1950).
- ²⁴P. G. De Gennes and P. A. Pincus, *Solid State Commun.* 7, 339 (1969).
- ²⁵J. Kaczer, M. Zeleny, P. Suda, *Czech. J. Phys. B* 13, 579 (1963).
- ²⁶C. Kittel, *Phys. Rev.* 70, 965 (1946).
- ²⁷M. Abramovicz and I. A. Stegun, *Handbook of Mathematical Functions* (Dover, New York, 1965).
- ²⁸P. M. Morse and H. Feshbach, *Methods of Theoretical Physics* (McGraw-Hill, New York, 1953) Vol. I.
- ²⁹A. Janossy and P. Monod (private communication).
- ³⁰J. Miltat (private communication).
- ³¹L. Schön and U. Buchenau, *Int. J. Magn.* 3, 145 (1972).
- ³²P. J. Grundy, D. C. Hothersall, G. A. Jones, B. K. Middleton, and R. S. Tebble, *Phys. Status Solidi A* 9, 79 (1972).